Configurational statistics in a-$Si_xN_yH_z$ alloys: A quantitative bonding analysis

E. Bustarret, M. Bensouda, M. C. Habrard, and J. C. Bruyère
Laboratoire d'Etudes des Propriétés Electroniques des Solides du Centre National de la Recherche Scientifique, Université Joseph Fourier, Grenoble, Boîte Postale 166, 38042 Grenoble Cédex, France

S. Poulin
Département de Génie Electrique, Ecole Polytechnique de Montréal, Case Postale 6079 Succursale A, Montréal (PQ), Canada H3C 3A7

S. C. Gujrathi*
Laboratoire de Physique Nucléaire, Université de Montréal, Case Postale 6128 Succursale A, Montréal (PQ), Canada H3C 3J7
(Received 7 December 1987)

The composition of hydrogenated silicon nitride films produced either by plasma-enhanced chemical-vapor deposition (PECVD) with $0.01 \leq [NH_3]/[SiH_4] \leq 20$ in the 220–320-°C temperature range or by low-pressure chemical-vapor deposition at 800 °C was determined by elastic-recoil-detection techniques and compared with the relative and absolute atomic densities deduced from x-ray photoelectron spectroscopy and optical measurements in the infrared (ir) range. The [N]/[Si] ratio of PECVD samples followed a square-root dependence on $[NH_3]/[SiH_4]$ over most of the gas-ratio range. We propose original calibrations of most of the ir-absorption bands observed in these samples over the 600–3600-cm^{-1} range, and we derived the experimental bond statistics by assuming complete valence satisfaction. In particular, the oscillator-strength factor of each of the six components of the SiH stretching peak was determined. The detailed statistics of all the hydrogenated configurations established for the first time in such a silicon-based ternary alloy are then compared to those expected to those expected for a random-bonded network. The most striking deviations from configurational randomness were observed at low nitrogen contents where more than two out of three silicon neighbors of a given nitrogen atom are monohydrogenated. Nitrogen atoms are found to have at least one monohydrogenated silicon nearest neighbor in all samples up to $[N]/[Si] = 1.1$. The generality of such a second-neighbor correlation in hydrogenated III-IV amorphous alloys is also discussed.

I. INTRODUCTION

Even though the knowledge of absolute atomic and bond concentrations in silicon-based unhydrogenated amorphous alloys was found to be sufficient for the semiempirical extrapolation of some basic optical constants at a given wavelength,[1–3] or for the calculation of model electronic band profiles,[4] it is now generally admitted[4–7] that the statistics of silicon tetrahedra and the specific electronic features of each of these first-neighbor configurations must be considered when spectroscopic properties are to be accurately described. This was first pointed out by Philipp,[5] who used the binomial statistics of silicon-centered tetrahedra in order to describe quantitatively the random character of a-SiO_x (Ref. 5) and a-SiN_y (Ref. 6) binary alloys. Further studies[7] showed that Philipp's approach was partly inadequate because the dielectric properties of microscopically heterogeneous media are not a simple statistically weighted linear superposition of the dielectric functions of these tetrahedra. Quite satisfying results were obtained on a-SiO_x and a-SiN_y systems,[7] as well as on a-SiO_xN_y materials[8] when the microscopical heterogeneity of the dielectric was taken into account.

To our present knowledge, the basic assumption of Philipp's random-bond model (RBM), according to which the tetrahedra distribution followed a bi- or multinomial patter, has rarely been tested in detail. Experimental attempts to estimate these statistics involved the decomposition of Si $2p$ core-level x-ray photoelectron spectra (XPS) of both a-SiO_x (Ref. 9) and a-SiN_y (Ref. 10) alloys into five equally spaced lines at fixed energies. In the case of amorphous silicon nitrides, this procedure is still subject to controversy[11,12] and permanent-charge-transfer calculations[13] have shown that the peak energy of each Si $2p$ core-level photoemission component depended on the film composition, so that the decomposition of the XPS peak is not straightforward. The Si $2p$ core-level spectra may, however, yield crucial information about the chemical order on an atomic scale, provided the experiment is properly conducted: for example, a biphasic (a-Si/a-Si_3N_4) system could be observed on a-SiN_y films evaporated *in situ*.[14] In this somewhat exceptional case, the lack of signal at intermediate binding energies provided experimental evidence for short- and medium-range segregation between pure a-Si and a-Si_3N_4 regions which must nevertheless be connected somehow: such a long-range ($Si\,Si_4$)/($Si\,N_4$) separation and the bino-

mial statistics are merely two extreme reference cases of chemical order and disorder, respectively.

When hydrogen is also present in the above-mentioned silicon-based continuous random networks (CRN's), a wealth of additional first-neighbor configurations appear so that the extent and pattern of the chemical order will depend critically on the preparation parameters.[15] Specific deposition conditions may, for example, lead to the synthesis of new materials such as amorphous polysilane polymers[16] a-$(SiH_2)_n$ or to the silicon diimide[17] a-$Si(NH)_2$. Also, the spatial correlations between bonded hydrogen and impurities or structural defects which have been observed in both doped[18,19] and undoped[20] a-Si:H films are essential features of current models of these materials.[21,22] Finally, the preferential incorporation of hydrogen from the ammonia observed in plasma-enhanced chemical-vapor-deposited (PECVD) amorphous hydrogenated (or deuterated) silicon nitrides[23] has been connected both to hydrogenated nitrogen precursors[24] for solid film growth and to the strong structural distortions that could be accommodated by hydrogenated units (either on Si or N) because of their lower coordination to the matrix.[13]

It is the aim of the present study to establish experimentally original first-neighbor statistics of both nitrogen and hydrogenated silicon atoms for a set of nonstoichiometric PECVD a-$Si_xN_yH_z$ samples prepared at $[NH_3]/[SiH_4]$ ratios ranging from 1/100 to 20/1. In order to derive these configurational distributions, we shall compare in the next section various experimental determinations of the [N]/[Si] ratio of these films. A detailed study of the ir-absorption spectra of these $\sim$1-μm-thick samples will then be presented in Sec. III. Elastic-recoil-detection[25] (ERD) profiles of a second set of thinner nearly stoichiometric films ([N]/[Si]$\approx$4/3) grown at different temperatures provided an absolute calibration of the ir-absorption bands which will be presented in Sec. IV, along with the complete quantitative bonding analysis resulting from valence satisfaction in both sets of samples. Section V will focus on the comparison between our experimentally derived configurational statistics and those associated with ideal random bonding for [N]/[Si] ratios from 0.03 to 1.4. The possible origins of the observed preferential bonding sites will also be discussed in this section. Finally, the highlights of our work will be summarized in Sec. VI, where our results will be compared to experimental data obtained on other silicon-based amorphous hydrogenated alloys.

Most of the preparation and characterization techniques used for the present study are already well known for a-Si:H–related materials. Relevant references and experimental details will be given when necessary along with the analysis of the results.

II. EXPERIMENTAL DETERMINATIONS OF THE [N]/[Si] RATIO OF NONSTOICHIOMETRIC SAMPLES

Excluding the calibrated ir spectroscopy, which will be discussed at length in the following sections, most of the experimental techniques leading to [N]/[Si] values in a-$Si_xN_yH_z$ alloys of varying densities can be classified in three categories.

(i) Direct measurements involving massive-particle detection, for instance, ERD,[26,27] or the more popular Rutherford backscattering spectroscopy (RBS).[2,27–30]

(ii) Electronic probes such as Auger-electron spectroscopy (AES),[3,31,32] XPS core-level analysis,[10,33] and electron microprobe analysis (EPMA).[34–36]

(iii) Indirect estimations based on the [N]/[Si]-sensitive and monotonic variations of an easily measurable physical quantity, for example the refractive index at a given wavelength.[1–3]

In this short section we shall compare these three methods through measurements which were performed on a first set of 1-μm-thick a-$Si_xN_yH_z$ films deposited at 320 °C in a capacitively coupled 50-kHz PECVD reactor described elsewhere[26] at $[NH_3]/[SiH_4]$ ratios ranging over more than 3 orders of magnitude. The silane was 1:9 diluted in hydrogen, and the total pressure was kept constant at 250 Pa. The power density (0.2 W cm^{-2}) was lower than that of a recent study at the same discharge frequency.[2] Both monocrystalline silicon and fused-silica double-polished substrates were introduced in each run.

For nitrogen and silicon elastic-recoil detection, the usual ERD setup[25,27] where the mass discrimination is obtained by Mylar foils was substituted by a more reliable time-of-flight measurement.[37] The resulting accuracy on both the [N]/[N + Si] and [H]/[H + Si] ratios was better than 5%. The results of ^{35}Cl ERD time-of-flight analysis of this set of samples are represented in Fig. 1 as a function of the gas ratio. The present [N]/[Si] ERD values are lower than those of a previous and more limited study[26] because a new calibration procedure on thinner samples reduced the experimental [N]/[N + Si] values by 10%.

The values of the refractive index at 0.6328 and 4 μm were deduced, respectively, from ellipsometry measurements and from the fringe pattern of the ir-transmission spectra of films deposited on crystalline silicon substrates. They are shown in Fig. 2 to be in fair agreement with the static index values deduced from the transparence region of the optical-absorption spectra of similar films deposited on fused silica. It has been proposed[1] that the refrac-

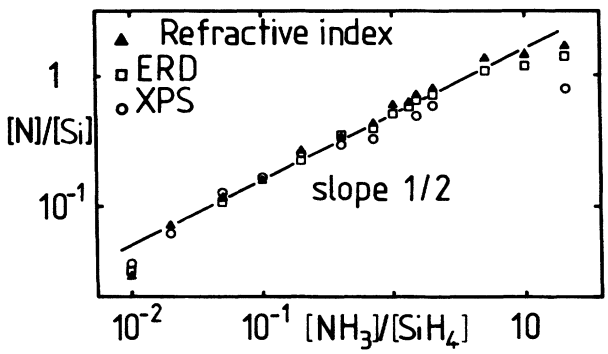

FIG. 1. Solid-state [N]/[Si] ratio vs $[NH_3]/[SiH_4]$ gas ratio for a-$Si_xN_yH_z$ PECVD films as deduced from static refractive-index values, elastic-recoil-detection analysis, and x-ray photoelectron spectroscopy $A_{Ni\,1s}/A_{Si\,2p}$ area ratios.

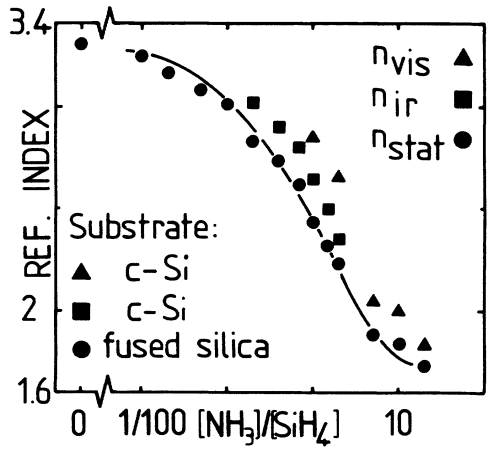

FIG. 2. Refractive indices of a-$Si_xN_yH_z$ films measured at 0.6328 μm (n_{vis}), around 4 μm (n_{ir}), and in the static limit (n_{stat}) as a function of the $[NH_3]/[SiH_4]$ gas ratio.

tive index of a-$Si_xN_yH_z$ alloys could be represented as the bond-density–weighted linear combination of reference refractive indexes taken at $y=0$ and at $y/x=4/3$, according to

$$n=\frac{[\text{Si—N}]n_{a\text{-}Si_3N_4}+[\text{Si—Si}]n_{a\text{-Si:H}}}{[\text{Si—N}]+[\text{Si—Si}]}\ , \tag{1}$$

where [Si—N] and [Si—Si] are absolute bond densities per unit volume. If hydrogen bonding is neglected in a-$Si_xN_yH_z$ films, this expression becomes[1]

$$n=\frac{n_{a\text{-Si:H}}+(3y/4x)(2n_{a\text{-}Si_3N_4}-n_{a\text{-Si:H}})}{1+3y/4x}\ . \tag{2}$$

For $y/x\approx 1$, a linear expansion of this last expression yields the experimentally observed linear relationship between the refractive index and either the [N]/[Si] (Ref. 3) or the [Si]/[N] (Ref. 2) ratios. In a more general way, since reference indexes are experimentally available, Eq. (2) provided a simple determination of y/x in films of known index.

Another possibility is to deduce the XPS $A_{N\,1s}/A_{Si\,2p}$ area ratio from core-level spectra obtained on these films either with the Al $K\alpha$ or the Mg $K\alpha$ excitation lines and reported in detail elsewhere.[13] These area ratios were then corrected[38] for the transmission function of the spectrometer, the photoelectronic cross sections, and the electron mean free paths λ associated with these two core levels. We chose to use the global correction factor of 0.509 proposed by Nefedov[39] for the Al $K\alpha$ line, which corresponded to $\lambda(\text{N }1s)=15.1$ Å taking confirmed cross-section values[40] and assuming $\lambda(\text{Si }2p)=21.6$ Å as deduced[41] from a Bohr radius $r_s(\text{Si }2p)=0.276$ Å[42]. The Mg $K\alpha$ data were processed in a similar way, and the resulting [N]/[Si] ratios are compared in Fig. 1 to those derived from experimental static index values according to Eq. (2) with $n_{a\text{-Si:H}}=3.3$ and $n_{a\text{-}Si_3N_4}=1.9$.

At low gas ratios the agreement between the three measurements is quite satisfactory. Above $[NH_3]/[SiH_4]=1/2$, the [N]/[Si] ratios deduced from XPS and refractive-index measurements are systematically higher and lower, respectively, than those determined by ERD analysis. The latter is the most reliable in this stoichiometry range, as shown in the next section. A better agreement of the data extracted from the refractive index with ERD results would, of course, be achieved at high gas ratios if the lower static index of our nearly stoichiometric 20/1 sample were used as $n_{a\text{-}Si_3N_4}$ in Eq. (2). In this case the resulting accuracy of this "calibrated" semiempirical procedure for the determination of [N]/[Si] in a-$Si_xN_yH_z$ films is rather striking. As for the discrepancy between ERD and XPS determinations, it is probably a result of the variation of the mean-free-path ratio $\lambda(\text{N }1s)/\lambda(\text{Si }2p)$ with composition, and it shows that an experimental correction factor estimated on a stoichiometric a-Si_3N_4 sample may not be valid at low nitrogen contents, since $\lambda(\text{Si }2p)$ reaches 30 Å in this material.[43] Finally, the linear part of the log-log plot of Fig. 1 yields a square-root dependence of the [N]/[Si] ratio on the $[NH_3]/[SiH_4]$ ratio in the 2/100 to 5/1 range, which is typical of an $AB\leftrightarrow A+B$ rate-limiting step which could involve, for instance, triaminosilane ions.[44] The observed dependence is stronger (slope ≈ 1) at lower gas ratios, in agreement with the linear behavior reported for $2\times10^{-5}\leq[NH_3]/[SiH_4]\leq 8/100$ in rf PECVD films[35] and with the respective slopes of 0.8 and 1.1 obtained in plots similar to Fig. 1 for PECVD [13.56 MHz (Ref. 45) and 50 kHz (Ref. 46), respectively] boron- and phosphorus-doped a-Si:H.

III. INFRARED-ABSORPTION SPECTROSCOPY OF NONSTOICHIOMETRIC SAMPLES

The ir-absorption spectra $\alpha(\omega)$ between 300 and 1300 cm^{-1} shown in Fig. 3 were deduced from room-temperature relative transmission measurements in the 300–4000-cm^{-1} range in a manner detailed elsewhere.[13] The dominant features of the a-Si:H spectrum in the 300–500-cm^{-1} range, at 630 and 875 cm^{-1}, respectively, attributed to disorder-induced silicon matrix modes, to local SiH wag-rocking (w-r) vibrations, and to SiH_2 bending (b) motions are progressively smeared out as the two broad bands around 470 and 850 cm^{-1} associated

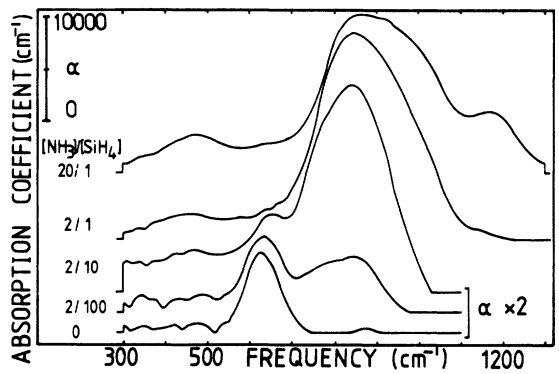

FIG. 3. ir-absorption spectra of a-$Si_xN_yH_z$ alloys deposited at various $[NH_3]/[SiH_4]$ ratios by PECVD.

with SiN symmetric and asymmetric stretching (st) modes increase with nitrogen incorporation.

The main results of a specific study of hydrogen-related local vibrational modes in this same set of samples which has been reported elsewhere[13] are summarized in Fig. 4. As a first approach, the normalized integrated absorption intensities $I_{\text{bond (mode)}} = \int_{\text{band}} \alpha\omega^{-1} d\omega$ of both SiH- and NH-related absorption lines were plotted against the $[NH_3]/[SiH_4]$ gas ratio, without any decomposition of the bands. In the case of silicon-hydrogen bonds, the wag-rocking-, bending-, and stretching-mode peak wave number shifted, respectively, from 630 to 660 cm,$^{-1}$ from 875 to 945 cm^{-1}, and from 2005 to 2185 cm^{-1} when $[NH_3]/[SiH_4]$ increased from 0 to 20. It should be noted that the stretching and wag-rocking band intensities do not scale and that SiH_2 bending motions are detected at all compositions.

The NH stretching-mode absorption band detected around 3300 cm^{-1} at gas ratios as low as 5/100 shifts to 3335 cm^{-1} at higher nitrogen contents. The much broader wag-rocking band can be resolved only at much higher $[NH_3]/[SiH_4]$ values and appears at 1175 cm^{-1} as a high-energy shoulder of the asymmetric stretch SiN main peak (see samples deposited at ratios 2/1 and 20/1 of Fig. 1). For gas ratios of 10/1 or 20/1, a narrow band around 1540 cm^{-1} was ascribed to NH_2 bending motions. Other weaker bands associated with NH_2 sites and also detected in these two samples[13] are not mentioned in Fig. 4.

Another result of our local-mode study[13] is that the SiH stretching band could best be described over the whole composition range as the sum of six Gaussian contributions of constant width to which first-neighbor configurations were assigned on the basis of original permanent atomic-charge calculations.[13] The peak frequencies and assignments of these components are given in Fig. 5 along with the variations of their normalized integrated absorption intensities against the $[NH_3]/[SiH_4]$ ratio. As it is mainly on the basis of this figure that we shall establish in Sec. V the configurational statistics of

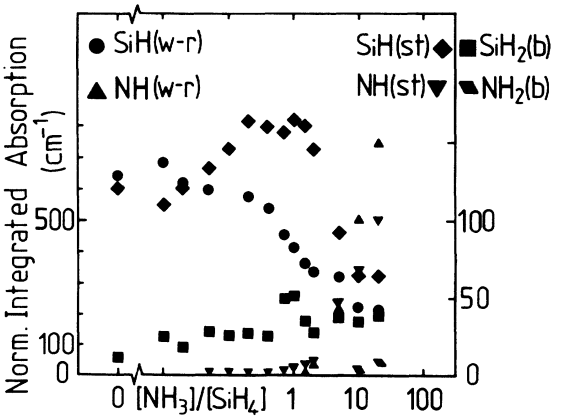

FIG. 4. Normalized integrated intensities of the main hydrogen-related vibrational modes observed by ir absorption as a function of the $[NH_3]/[SiH_4]$ gas ratio: stretching (st), bending (*b*), and wag-rocking (*w-r*).

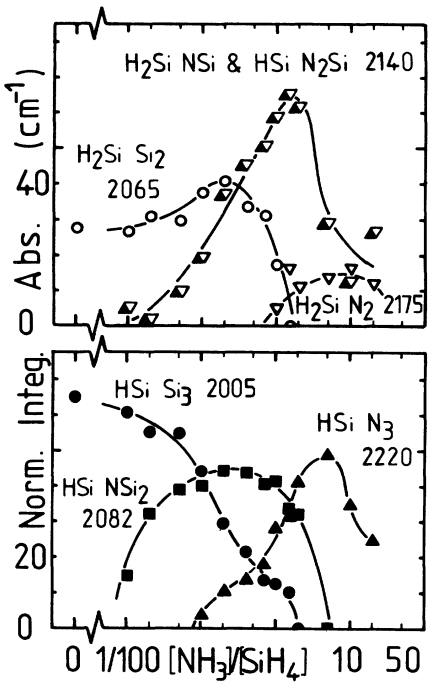

FIG. 5. Variations of the normalized integrated intensities of the six components of the Si—H stretching-mode absorption band with the gas ratio. The mean peak frequencies of the lines are given in cm^{-1} together with their assignments.

hydrogenated silicon atoms, we would like to point out that both the decomposition given here and the corresponding assignments[13] were corroborated by independent data published in the literature: in *a*-Si:H/*a*-$Si_xN_yH_z$ multilayers,[47] broader lines at 2080 and 2155 cm^{-1} were attributed to (HSi NSi_2) or (H_2Si Si_2) sites and (HSi N_2Si) or (H_2Si NSi) sites, respectively, while a decomposition into three Gaussian components at 2120, 2180, and 2255 cm^{-1} was necessary to interpret the annealing behavior of heavily hydrogenated, nearly stoichiometric *a*-$Si_xN_yH_z$ films.[48] We shall see in Sec. IV that up to three Gaussian lines may indeed be present in the spectra of nearly stoichiometric layers deposited between 200 and 800 °C. However, in our laboratory, the component at 2250 cm^{-1} which was attributed to the H_3SiN configuration[48] has not been observed in PECVD samples deposited above 200 °C.

The subtraction of the absorption bands related to hydrogen local motions (see Fig. 4 and Ref. 13) from the initial absorption spectra of Fig. 3 yielded the difference spectra represented in Fig. 6. The magnified spectra of the nitrogen-free and 2/100 samples show how in the latter, disorder-induced Si—Si matrix absorptions bands and particularly that from the LA mode at 340 cm^{-1} are enhanced by nitrogen incorporation. At intermediate gas ratios, these bands mingle with the Si—N "symmetric stretching" and Si "breathing" modes,[17] while a broad shoulder develops near 570 cm^{-1}. At still higher nitrogen contents, the absorption band between 300 and 600 cm^{-1} resulted from less localized ir-active phonons of the silicon nitride matrix, and a comparison with the results

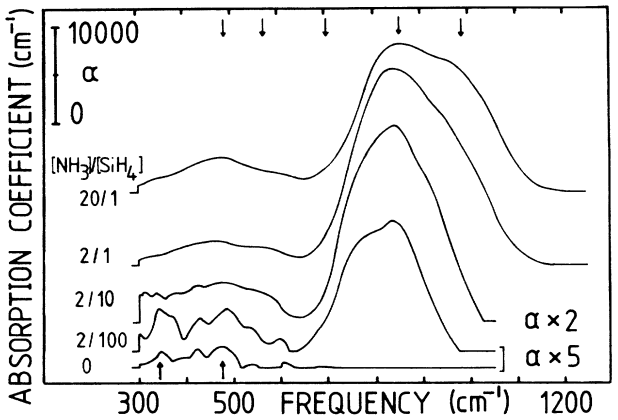

FIG. 6. Processed ir-absorption spectra of a-$Si_xN_yH_z$ samples resulting from the subtraction of all hydrogen-related local-mode absorption lines from the spectra of Fig. 3.

of a simplified dispersion analysis (where the interunit coupling was not taken into account) seemed justified: for a mixture of α and β phases in polycrystalline Si_3N_4, such an approach yielded two TO modes[49] in this spectral region, at 495 and 580 cm^{-1}. Because the peak absorption for our films lies rather in the 450–480-cm^{-1} range and because the 570-cm^{-1} shoulder is rather intense in our spectra,[50] we may moreover describe qualitatively the short-range order of nitrogen in these samples as being "close to" the (N Si_3) planar configuration observed in the β phase of crystalline Si_3N_4.[51]

The β-like character of the 20/1 sample is further confirmed in Fig. 6 by the high-energy profile of the main absorption peak, above 1040 cm^{-1}, which closely resembles that of β-Si_3N_4.[50,51] Also, the strong shoulder in the 970–1010-cm^{-1} range for this sample might be compared to the absorption lines at 996 (1001) cm^{-1} which have been observed in gaseous and liquid[52] (solid[53]) trisilylamine molecules where the (N Si_3) configuration is planar.

Let us now focus on the main peak around 850 cm^{-1}, which is generally attributed to the asymmetric stretching mode of Si—N bonds.[17] The strong variations of its line shape with the ammonia-to-silane ratio show that a realistic decomposition of this absorption feature would involve at least three lines (see Fig. 6). Indeed, accurate dispersion analysis of conventional[54] and Fourier-transform[55] ir spectra yielded four (three) components at 820, 890, 940, and 1000 cm^{-1} (830, 900, and 970 cm^{-1}) for CVD (Refs. 54 and 55) [PECVD (Ref. 55)] nearly stoichiometric films. However, neither these lines nor the 840-cm^{-1} (970-cm^{-1}) component associated with isolated (clustered) (N Si_3) sites in nonhydrogenated a-SiN_y ($y > 0.15$) films could explain the low-energy shoulder clearly observed in our samples deposited at low $[NH_3]/[SiH_4]$ ratios (see Fig. 6). This shoulder around 760 cm^{-1} is similar to the broad absorption band observed in unannealed heavily N_2^+-implanted silicon,[56] which displayed a maximum below 800 cm^{-1}. Also, a much narrower line at 764 cm^{-1} reported for lower nitrogen implantation doses in crystalline silicon[57] has been attributed to silicon-vacancy-related configurations of the isolated nitrogen atom. We shall therefore ascribe this shoulder to nitrogen sites where both the Si—N bonds and the local silicon network are strongly distorted.

A last absorption feature, which has been numerically detected in a systematic manner for gas ratios greater than 1/1, is hardly to be seen in the same region of the spectra of Fig. 6. Since the intensity of this weak component centered in the 690–710-cm^{-1} range rose markedly in the spectra of the 5/1, 10/1, and 20/1 samples, we tentatively assigned it to the coupled breathing motion of bridging NH units.[58]

Finally, it is striking that the peak frequency of the main SiN absorption band remained almost unaffected at 845 ± 3 cm^{-1} throughout the 1/100 to 2/1 gas-ratio range, while its shape and intensity varied quite drastically, as detailed above. This is illustrated in Fig. 7, which shows the variations of the peak position. The maximum absorption and the normalized integrated absorption also shown in this figure follow similar but not quite parallel trends with increasing $[NH_3]/[SiH_4]$ values. For gas ratios greater than 2/1, the frequency of the absorption peak rose to 865 cm^{-1}. This is a result of the increasing NH concentration (while the Si—H bond density decreased) in our alloys, as previously and unambiguously demonstrated on SiH-free silicon diimide films.[17]

IV. QUANTITATIVE BONDING ANALYSIS

A. Continuous covalent networks

For any chemically bonded covalent system, a general relationship between the absolute concentration $[A_\alpha^i]$ of an α-coordinated atom of type i and the densities of chemical bonds $[A_\alpha^i - A_\beta^j]$ involving this atom in an α-coordinated site is

$$\alpha[A_\alpha^i] = \sum_{i \neq j, \alpha \neq \beta} [A_\alpha^i - A_\beta^j] + 2[A_\alpha^i - A_\alpha^i] \, . \tag{3}$$

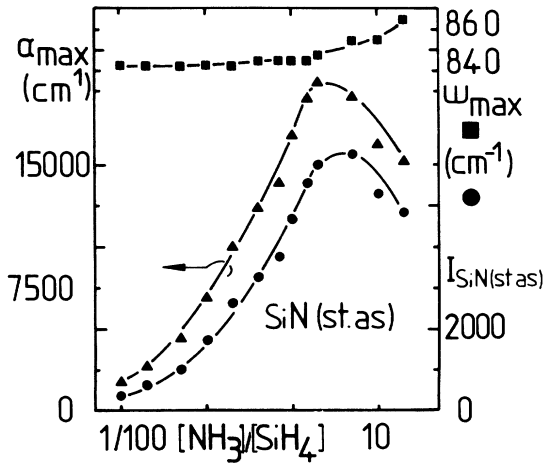

FIG. 7. Peak frequency, maximum absorption, and normalized integrated intensity of the Si—N asymmetric stretching-mode (st. as.) absorption band as a function of the $[NH_3]/[SiH_4]$ gas ratio.

The resulting group of equations which describe the system become simpler if the network is assumed to be continuous, so that the concentration of molecular species (for instance H_2, N_2, or O_2 in voids) is negligible. Blister-free gas evolution and annealing studies[36,59] confirmed that this was indeed the case in a-$Si_xN_yH_z$ alloys, and indicated, moreover, that single or multiple N—N bonds were not likely to occur in these samples. Since ESR studies[60] showed also that the proportion of Si (N) atoms with a coordination different from 4 (3) was in (below) the ppm range in our films, we may derive from Eq. (3) the following set of equations:

$$[H]=[Si—H]+[N—H]\ , \tag{4}$$

$$3[N]=[Si—N]+[N—H]\ , \tag{5}$$

$$4[Si]=[Si—N]+[Si—H]+2[Si—Si]\ . \tag{6}$$

The resulting influence of hydrogen bonding on both the [N]/[Si] and [H]/[Si] ratios of nearly stoichiometric films is represented in Fig. 8. The assumption that both the [Si—Si] and [N—N] bond densities are negligible introduced forbidden regions in the [N]/[Si]-versus-[H]/[Si] plane, while Eqs. (4)–(6) defined bundles of converging (parallel) straight lines when only the parameters a or b (c) defined in Fig. 8 vary. The obvious effect of a rising [N—H] ([Si—H]) bond density is to enhance (decrease) the [N]/[Si] ratio within boundaries which expand with increasing hydrogen contents. Furthermore, some regions of the plane can be reached only if specific hydrogenated configurations are present: SiH_2 and SiH_3 sites for $c>1$ and $c>2$, respectively, and NH_2 terminals if $b>1$, for instance. Finally, if the N—N bond concentration can be neglected in any silicon nitride system, the $a=1$ frontier of Fig. 8 provides an upper limit for [N]/[Si] values of all a-$Si_xN_yH_z$ alloys as a function of their hydrogen contents. It should be stressed that in off-stoichiometry samples where Si—Si bonds are present distinct (b,c) pairs may lead to the same composition, whereas this is impossible in Fig. 8.

B. Bonding analysis of nearly stoichiometric films

For films thinner than 0.8 μm, the presence of the ERD signal corresponding to the crystalline-silicon substrate provides an absolute calibration of the atomic-silicon concentration $[Si]_{sub}$, as shown in Fig. 9, where the atomic density profiles of typical PECVD and LPCVD films were represented.

In order to calibrate the most reliable ir-absorption bands with ERD results, we studied a second set of thinner nearly stoichiometric ($[N]/[Si]\approx 4/3$) samples deposited either by PECVD under conditions similar to those described above or by LPCVD in an industrial production chamber, as detailed in Table I. Samples 1–3 were deposited under identical conditions but during various deposition times, and substrate-holder temperatures ranged from 220 to 800 °C.

The maximum absorption in the spectra of the PECVD samples was observed around 860 cm^{-1}, while that of the LPCVD sample occurred at a frequency of 845 cm^{-1}. The Si—H stretching band of these samples contained up to three components at 2140, 2175, and 2220 cm^{-1}, and a high-energy shoulder was observed at about 3445 cm^{-1} in the N—H stretching-mode absorption profile. The integrated intensity of this Gaussian component was found to scale by a factor of $\frac{4}{3}$ with that of the NH_2 bending mode line near 1540 cm^{-1} (see Fig. 10) and this absorption shoulder was thus ascribed to an unresolved NH_2 stretching mode doublet also observed by other authors.[61,62] The normalized integrated intensities of the above-mentioned bands, as well as that of the NH (wagrocking) mode near 1175 cm^{-1} are given in Table II for the six samples of this second set. The main uncertainty on these values came from the thickness measurements and inhomogeneties, and it was of the order of 10%. These results were compared to the mean atomic densities (obtained by ERD and given in Table III) through Eqs. (4)–(6). The calibration factors verifying $[A—B]=K_{AB\,(\mathrm{mode})}I_{AB\,(\mathrm{mode})}$ were deduced from a best-fit procedure on all three equations by assuming all Si—Si bonds to occur only on the hydrogenated sites which give

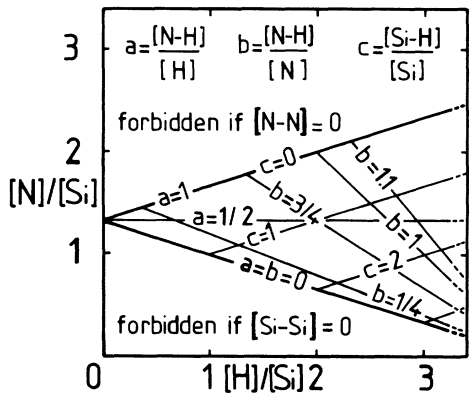

FIG. 8. Influence of the hydrogen-to-silicon concentration ratio on [N]/[Si] in a covalent continuous a-$Si_xN_yH_z$ alloy described by Eqs. (4)–(6).

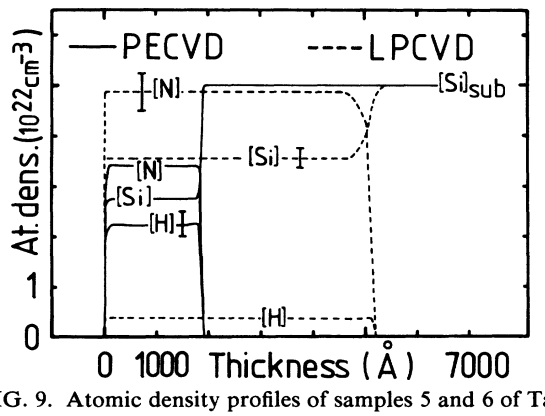

FIG. 9. Atomic density profiles of samples 5 and 6 of Table I as deduced from elastic-recoil-detection analysis. The concentration of the monocrystalline silicon substrate $[Si]_{sub}$ provided the absolute density scale.

TABLE I. Preparation conditions and thicknesses of nearly stoichiometric a-$Si_xN_yH_z$ films deposited on monocrystalline-silicon substrates.

	Sample					
	1	2	3	4	5	6
Thickness (Å)	900	1950	3200	3700	1900	5200
T_s (°C)	320	320	320	320	220	800
$[NH_3]/[SiH_4]$	10/1	10/1	10/1	20/1	10/1	LPCVD

rise to the Si—H stretching absorption component at 2140 cm^{-1} (see Table II). The values for K_{AB} are given in the lowest line of Table II. It is striking that the fit on the nitrogen contents which involved two independent factors [for the SiN main absorption band and the NH(w-r) shoulder, respectively] should yield the same value at 2.07×10^{19} cm^{-2} for both factors. This value is, moreover, quite close to that of the oscillator strength factor of the local SiN asymmetric stretch of N-doped floating-zone crystalline silicon[63] observed at 963 cm^{-1} (2.1×10^{19} cm^{-2}), but much higher than another value proposed for various amorphous alloys[64] with $[N]/[Si]\leq0.3$ (2.9×10^{18} cm^{-2}). Taking into account the common calibration factor of Table II, one may furthermore write Eq. (5) as

$$[N]=C_N\int_{\approx700}^{\approx1300}\alpha\omega^{-1}d\omega\ , \tag{7}$$

where

$$C_N=\tfrac{1}{3}K_{SiN\ (st.as.)}=\tfrac{1}{3}K_{NH\ (w\text{-}r)}=6.9\times10^{18}\ cm^{-2}\ .$$

This calibration factor C_N is in fair agreement with the value of 7.7×10^{18} cm^{-2} proposed for CVD films,[65] where the absolute silicon density was assumed to drop linearly between 5×10^{22} cm^{-3} at $y=0$ and 4×10^{22} cm^{-3} at $y/x=4/3$. More indirect estimations[56,66] yield a higher value for C_N at 9.2×10^{18} cm^{-2} in implanted films, while a similar constant of 6.7×10^{18} cm^{-2} has been recently deduced for PECVD films in the $0\leq y/x\leq0.9$ range[24] from EPMA measurements.

We should make it clear that the above value of $K_{SiN\ (st.as.)}$ applies only to the restricted $1.25\leq[N]/[Si]\leq1.45$ range. $K_{SiN\ (st.as.)}$ is only the empirical calibration factor of a complex phonon-related absorption band, whereas the other K values proposed in Table II are true oscillator strength factors because they are associated with true local modes. Since our simultaneous fitting procedure of Eqs. (4)–(6) limited error propagation, we believe these values to be correct within 10%. The oscillator strength factors of the three Si—H stretching bands are given in Table II. They are of the same order of magnitude as the mean value reported for a-SiH (Ref. 67) at 1.4×10^{20} cm^{-2} but higher than the 3×10^{19} cm^{-2} proposed in an early study specific to a-$Si_xN_yH_z$ alloys,[68] which disagrees with most of the later estimations[69–71] around 10^{20} cm^{-2}.

Finally, even though the [N]/[Si] ratios of Table III are the same in samples 1–3, it is clear from Table II that higher concentrations of NH bonds are observed in thinner films (although these have slightly lower total hydrogen contents), pointing out to the role of NH units as stress relievers near interfaces.

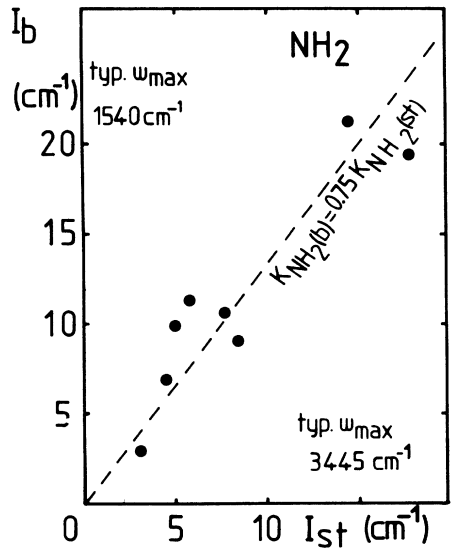

FIG. 10. Correlation between the normalized integrated intensities of the NH_2 stretching component (I_{st}) and of the NH_2 bending absorption band (I_b).

C. Bonding analysis of nonstoichiometric films

As stated above, all but two samples described in Secs. II and III were too thick for a direct determination of their absolute atomic densities. In the case of the quasi-stoichiometric layer deposited at $[NH_3]/[SiH_4]=20/1$, the [N—H], [Si—H], and [Si—N] bond densities could, however, be deduced from the ir-absorption spectrum and from the factors of Table II, and an approximate composition was found to be a-$Si_{0.3}N_{0.4}H_{0.3}$. In order to derive the absolute silicon concentration of our non-stoichiometric alloys, we propose to write of the multilinear bond-density dependence of the refractive index observed in various silicon-based alloys[1,72,73] in a more general way than that of Eq. (1) by

$$n_{stat}-1=\gamma[Si—N]+\delta[Si—Si]\ . \tag{8}$$

Introducing the atomic densities through Eqs. (5) and (6), the absolute silicon concentration is then given by

$$[Si]=\frac{n_{stat}-1+(\gamma-\delta/2)[N—H]+[Si—H](\delta/2)}{2\delta+3(\gamma-\delta/2)[N]/[Si]}\ . \tag{9}$$

TABLE II. Normalized integrated absorption (in cm^{-1}) and detailed assignments of reliable ir-absorption bands in nearly stoichiometric samples.

	ω_{max} (cm^{-1})					
Sample	845–870	1175	3445	2140	2175	2220
1	4700	480	6.8	6	1.1	10.9
2	4930	550	8.4	2.8	4.7	9
3	4850	340	3.2	7.8	11.1	24.4
4	4760	580	5.1	2.4	6.5	10.2
5	4100	420	9.9	10.2	17	28.1
6	7420	100				6.7
K (cm^{-2})	2.07×10^{19}	2.07×10^{19}	5×10^{20}	1.1×10^{20}	4×10^{20}	2×10^{20}
Mode	asym. stretch	wag-rock	stretch	stretch	stretch	stretch
Configuration	SiN	NH NH_2	NH_2	$HSiN_2Si$ H_2SiNSi	H_2SiN_2	$HSiN_3$

In our particular case, calibrations on our *a*-Si:H and *a*-$Si_{0.3}N_{0.4}H_{0.3}$ films yielded an approximate but simpler empirical formula:

$$[Si]\ (cm^{-3})=(1.35\times10^{22})n_{stat}+0.25[Si—H]\ . \quad (10)$$

The absolute nitrogen densities are then determined using the ERD results of Fig. 7, and are plotted along with the silicon concentrations from Eq. (10) in Fig. 11 as a function of the solid-phase [N]/[Si] ratio. The agreement with ERD results for a 0.7-μm-thick intermediate ([N]/[Si]=0.11) sample was excellent. The hydrogen atomic densities also given in Fig. 11 were deduced from NH and SiH nonshifting stretching absorption lines (using the oscillator strength factors of Table II) and from the additional absolute ERD data on the two thinner samples deposited at low 1/100 and 5/100 $[NH_3]/[SiH_4]$ ratios as well as from earlier nuclear measurements on the nitrogen-free sample. The corresponding oscillator-strength factors for the Si—H stretching-mode components at 2005, 2065, and 2082 cm^{-1} (see Fig. 5) were 7, 11, and 17×10^{19} cm^{-2}, respectively, while $K_{NH\ (st)}=(12\pm3)\times10^{19}$ cm^{-2}. The semilogarithmic plot of Fig. 11 shows that the hydrogen contents are maximum in the $0.4\leq[N]/[Si]\leq0.7$ range, and that the concentration of silicon atoms is roughly linear with [N]/[Si], as proposed earlier.[65] At [N]/[Si] ratios greater then 0.7, the results are obviously preparation dependent, and our data do not follow the general trend of a total mass density increasing with [N]/[Si],[68,74–76] probably because of the high concentrations of NH and NH_2 units in our nearly stoichiometric samples.

The variations of the Si—H and N—H bond densities with the [N]/[Si] ratio as given in Fig. 12 confirm the strong correlations between high density and high Si—H concentration on one hand and low density and high N—H contents on the other. Also in Fig. 12, the opposite variations of Si—Si and Si—N bond densities are strikingly symmetrical, while at [N]/[Si] ratios lower than 0.5, the additional hydrogen introduced in the layer along with nitrogen is bonded to silicon rather than to nitrogen. As most of the hydrogen of such PECVD alloys is known to come from the ammonia,[23] this tendency indicates that in our strongly bombarded 50-kHz samples hydrogen bonding in the solid phase results from surface or bulk rearrangement rather than from the gas-phase plasma chemistry, while the nitrogen incorporation was shown in Sec. III to be strongly related to the gas-phase composition (see Fig. 1).

Finally, the total Si—H and Si—N bond densities of Fig. 12 were compared to the normalized integrated intensities of the Si—H wag-rocking and of the Si-N asymmetric stretching absorption bands given in Figs. 4 and 7, respectively. The resulting "calibration" factors plotted in Fig. 13 are independent of the composition in limited ranges only. $K_{SiH\ (w\text{-}r)}$ is very strongly affected at low nitrogen contents, and is about constant at $7.8\pm0.4\times10^{19}$ cm^{-2} for $[N]/[Si]\geq0.6$, instead of $(1.6\pm0.1)\times10^{19}$ cm^{-2} in *a*-Si:H.[67] On the contrary, $K_{SiN\ (st.as.)}$ was found to be constant for $[N]/[Si]\leq0.8$ at about $(1.3\pm0.2)\times10^{19}$ cm^{-2}, and seemed to be strongly composition dependent in the range $1\leq[N]/[Si]\leq1.5$. The trends illustrated by

TABLE III. Experimental (ERD) and calculated nitrogen atomic density and composition ratios obtained from the data of Table II through Eqs. (4)–(6).

	[N] (10^{20} cm^{-3})		[N]/[Si]		[H]/[Si]	
Sample	Expt.	Fit	Expt.	Fit	Expt.	Fit
1	361	357	1.44	1.4	0.57	0.53
2	371	378	1.44	1.42	0.6	0.6
3	368	362	1.43	1.3	0.62	0.57
4	377	368	1.47	1.42	0.62	0.59
5	341	312	1.23	1.16	0.8	0.82
6	488	517	1.37	1.34	0.112	0.104

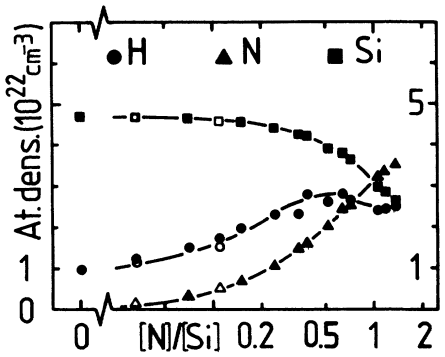

FIG. 11. Absolute atomic concentration in a-$Si_xN_yH_z$ as a function of the [N]/[Si] ratio. Open symbols correspond to direct ERD measurements.

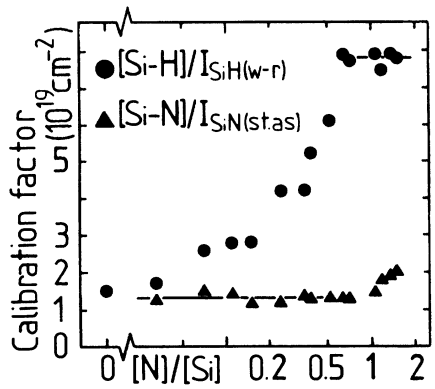

FIG. 13. Experimental calibration and oscillator-strength factors of the Si—N asymmetric stretching and Si—H wag-rocking modes as a function of the [N]/[Si] solid-state ratio.

Fig. 13 are quite similar to those of the peak frequencies of the two corresponding absorption bands, which were plotted against the $[NH_3]/[SiH_4]$ ratio, respectively, on Fig. 7 and in an other report.[13] The results confirm the general rule of ir quantitative bonding analysis, according to which the calibration of shifting lines is not at all straightforward, whether they correspond to local modes or not.

D. Random bonding and chemical order

In our silicon-nitrogen hydrogenated alloys, chemical order could promote the growth of many amorphous stoichiometric phases other than the obvious a-Si and a-Si_3N_4 references. If simple molecular species such as SiH_4, NH_3, $Si(NH_2)_4$, and $N(SiH_3)_3$ are excepted, a wealth of polymerlike (for instance, a-(SiH_2) or a-$[Si(NH_2)_2]$) or glassy materials [a-N(SiH), a-$N_2(SiH_2)_3$, or a-$Si(NH)_2$] remain to be considered. We have already stressed how the respective spatial dimensions of these phases could affect the bonding statistics, so that the existence of such heterogeneities could not be deduced from the experimental data of Figs. 11 and 12 alone.

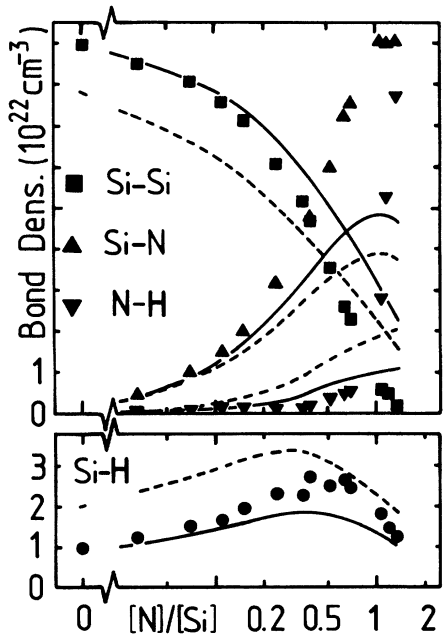

FIG. 12. Experimental bond densities in a-$Si_xN_yH_z$ alloys as a function of the [N]/[Si] solid-state ratio. The solid (dashed) line resulted from the application of Eqs. (14a) and (14b) [(12a) and (12b)] to our PECVD samples.

A more realistic approach is to compare the experimental bonding statistics to those expected for a random alloy. The random covalent model[77] has thus been opposed to chemically ordered network models[78] for the description of chalcogenides and glassy materials.[79] The former stipulated that the random-bond statistics of hypothetical alloy of total atomic and bond densities D and B (given, respectively, by $\sum_{i,\alpha}[A^i_\alpha]$ and $\sum_{i,\alpha}\alpha[A^i_\alpha]/2$) could be deduced from expanding the expression for B as follows:

$$B=\left[\sum_{i\neq j,\ \alpha\neq\beta}\beta[A^i_\alpha][A^j_\beta]+\sum_{i,\alpha}\alpha[A^i_\alpha]^2\right]\Big/2D\ . \tag{11}$$

Each of the terms of this expression was then identified with the density of each of the possible bonds in the network according to

$$[A^i_\alpha-A^j_\beta]=(\alpha+\beta)[A^i_\alpha][A^j_\beta]/2D \tag{12a}$$

and

$$[A^i_\alpha-A^i_\alpha]=\alpha[A^i_\alpha]^2/2D\ . \tag{12b}$$

However, such a definition is not compatible with Eq. (3) and must therefore be ruled out. We thus propose to derive the bond statistics of a random alloy by writing the expansion of B in an alternative way:

$$B=\left[\sum_{i\neq j,\ \alpha\neq\beta}\alpha\beta[A^i_\alpha][A^j_\beta]+\sum_{i,\alpha}\alpha^2[A^i_\alpha]^2\right]\Big/4B\ , \tag{13}$$

and to define the bond concentration associated with ideal randomness by

$$[A^i_\alpha-A^j_\beta]=\alpha\beta[A^i_\alpha][A^j_\beta]/2B\ , \tag{14a}$$

$$[A^i_\alpha - A^i_\alpha] = \alpha^2 [A^i_\alpha]^2 / 4B \ . \quad (14b)$$

These equations are compatible with Eq. (3), and have been recently applied to the specific case of SiN_x alloys.[3] Both models [resulting from Eqs. (12) and (14)] are compared to the experimental data on our a-$Si_xN_yH_z$ alloys in Fig. 12, and the results of the random covalent model (dashed lines) are shown to be quite different from those given by our random-bond covalent alloy (RBCA) model through Eqs. 14(a) and 14(b). Even though the lack of experimental evidence for H or N homopolar bonding was the main deviation from the ideal random character as defined by these equations, the bond statistics were those of a random alloy up to $[N]/[Si] \approx 0.2$. The experimental Si—H bond concentration was higher than that expected for the random case in the intermediate $0.2 \leq [N]/[Si] \leq 1.1$ range, a feature probably related to the structural constraints to be accommodated in this composition region where the concentration of NH bridging units was lower than expected within the random-bonding description. The structural relaxation brought to the network by the SiH and SiH_2 units[13] was taken over by the NH groups at $[N]/[Si] \geq 1$, as the concentration of the latter rose in a spectacular manner. This ammonia-related effect is, however, known to be preparation dependent,[17] and is not always observed when the Si-N concentration increases.

In order to investigate in more detail the apparent random character of our alloys at low nitrogen contents, we shall establish in the next section the statistics of the first-neighbor configurations (also called basic network formers[78]) which can be deduced from experiment. These will be compared to multinomial distributions based on the *experimental bond statistics of this section* rather than to those of the RBCA model, so that subtler second-neighbor correlation effects might not be hidden by the stronger and more general trends described above.

V. CONFIGURATIONAL STATISTICS

In order to obtain additional information about the random character of our continuous a-$Si_xN_yH_z$ alloys, we shall compare in this section the experimentally available configurational statistics to those expected for continuous random networks (CRN's).[80] In this approach, the randomness will be characterized by the statistical distribution of the 20 basic network formers that can be built on Si and N in amorphous hydrogenated silicon nitrides. The general definition of an ideal random-bonding network involves two hypotheses: First, the choice of p_{ij}, the elemental probability that an α-coordinated atom A^i_α of the system be bonded to an A^j_β atom; second, the assumption that the various first-neighbor configurations of A^i_α have probabilities which follow a multinominal law of order m, where m is the number of different atomic species present in the alloy, as proposed by various authors.[5,81,82] We propose here to define the elemental probability p_{ij} in a general way which is compatible with Philipp's specific approach of IV-II compounds:[83]

$$p_{ij} = \frac{[A^i_\alpha - A^j_\beta]}{\alpha [A^i_\alpha]} \quad \text{for } i \neq j \text{ or } \alpha \neq \beta \ , \quad (15)$$

$$p_{ii} = \frac{2[A^i_\alpha - A^i_\alpha]}{\alpha [A^i_\alpha]} \ . \quad (16)$$

For a given A^i_α central atom, the sum of p_{ii} and all p_{ij} probabilities is unity according to Eq. (3). In the particular case of a-$Si_xN_yH_z$ alloys, the probabilities for nitrogen-centered ($N\ Si_\mu\ H_\eta$) $(\mu+\eta=3)$ or silicon-tetrahedral ($Si\ Si_\mu N_\nu H_\eta$ $(\mu+\nu+\eta=4)$ basic formers will then be given by

$$p(N\ Si_\mu\ H_\eta) = \frac{3!}{\mu!\eta!} \frac{[Si—N]^\mu [N\text{-}H]^\eta}{(3[N])^3} \ , \quad (17)$$

$$p(Si\ Si_\mu N_\nu H_\eta) = \frac{4!2^\mu}{\mu!\nu!\eta!} \frac{[Si—Si]^\mu [Si—N]^\nu [Si—H]^\eta}{(4[Si])^4} \ , \quad (18)$$

where μ, ν, and η are integers between 0 and 3 [Eq. (17)] or 0 and 4 [Eq. (18)]. For the mono- and dihydrogenated silicon configurations detected by ir spectroscopy, the experimental site statistics deduced both from Fig. 5 and from the calibration procedure of Sec. IV were compared to those calculated through Eq. (18) in the various plots of Fig. 14.

At low nitrogen contents, the growth chemistry enhanced the concentration of (H_2 Si Si_2) sites and hindered the formation of (H Si Si_3) units in a way very similar to that observed in our nitrogen-free film. This is known to be a preparation-sensitive phenomenon and we

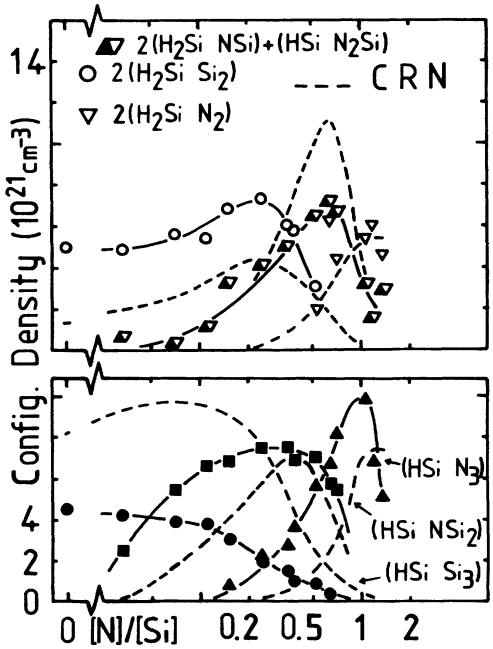

FIG. 14. Density of various hydrogenated silicon tetrahedra as a function of the [N]/[Si] ratio. The solid lines and symbols were deduced from Fig. 5. The dashed lines resulted from the application of Eqs. (15)–(18) to a-$Si_xN_yH_z$ alloys.

shall rather focus on the nitrogen-related trends observed in Fig. 14. Up to [N]/[Si]=0.3, the concentration of (H Si NSi_2) sites is much stronger than that expected for random bonding. At higher ratios ($0.15 \leq [N]/[Si] \leq 1.1$), the (HSi N_3) density is also much greater than expected, and the sums of (H_2 Si SiN) and (HSi SiN_2) concentrations are also in excess of the values calculated through Eq. (18). At still higher [N]/[Si] ratios the tendency reverses and all deviations from randomness become weaker for these hydrogenated silicon sites. A tentative separation of the (H_2Si SiN) and (HSi SiN_2) contributions to the 2140-cm^{-1} ir-absorption line based on the variations of the Si—H_2 bending-mode band intensity (see Fig. 4) enabled us to draw in Fig. 15 the relative fractions of unhydrogenated mono- and dihydrogenated silicon atoms as a function of the [N]/[Si] solid-phase ratio. It is striking that these quantities are almost equal to those predicted by the random-bonding model even though strong deviations from this model have been observed for the configurational statistics of Fig. 14. Up to [N]/[Si]=0.5, the small differences between the calculated and experimental site ratios of Fig. 15 follow quite clearly the trends observed in the nitrogen-free sample. At higher [N]/[Si] ratios no such systematic tendency could be determined. Finally, the variations of the concentrations of the five unhydrogenated silicon tetrahedra which resulted from Eq. (18) have been represented in Fig. 16. The most striking result of such a random-bond description of these sites was that the (Si Si_4) concentration was less than half its nitrogen-free value for [N]/[Si]=0.15. If this were indeed the case, it would mean that the strong distortions of the Si—Si bond angle observed in these alloys[84] affect primarily hydrogenated or nitrogenated tetrahedra.

Let us now focus on the configurational statistics related to nitrogen-centered basic formers. The respective fractions of nitrogen atoms in the (N Si_3), (HN Si_2), and (H_2N Si) sites are given in Fig. 17(a). They result from the chemical order affecting the bond statistics as described in the preceding section, and there was not any evidence for new effects as experimental and calculated values were within 5% of each other. Much more interesting information can, however, be extracted from the ir spectroscopy if one considers the data of Fig. 14 from the point of view of nitrogen second-neighbor configurations. The densities of nitrogen atoms, respectively, bonded to unhydrogenated, mono-, and dihydro-

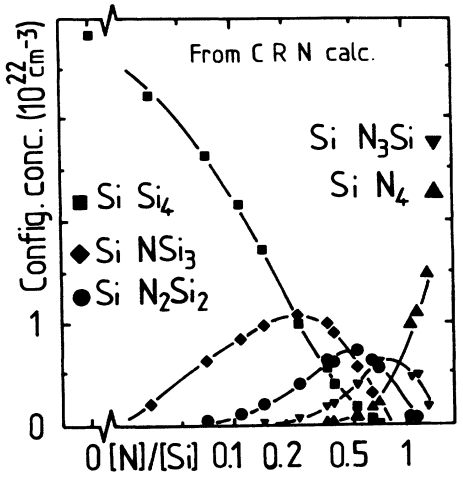

FIG. 16. Absolute density of unhydrogenated silicon tetrahedra deduced from Eqs. (15) and (16) as a function of the [N]/[Si] ratio.

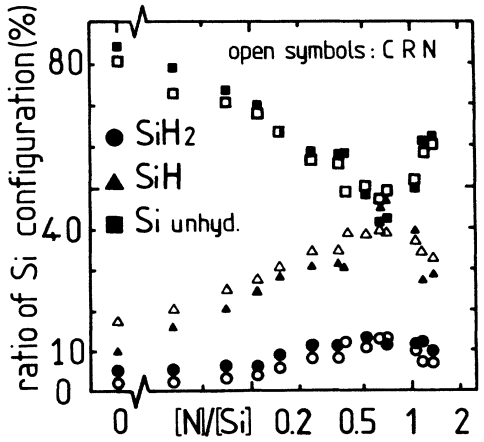

FIG. 15. Calculated (open symbols) and experimental fractions of unhydrogenated, monohydrogenated, and dihydrogenated silicon atoms in a-$Si_xN_yH_z$ alloys as a function of the [N]/[Si] ratio.

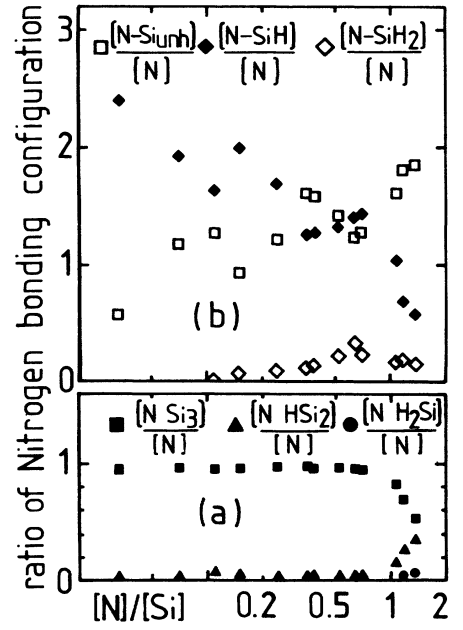

FIG. 17. (a) Experimental fraction of unhydrogenated, monohydrogenated, and dihydrogenated nitrogen atoms in a-$Si_xN_yH_z$ alloys as a function of the [N]/[Si] ratio. (b) Experimental mean number of unhydrogenated, mono- or dihydrogenated silicon neighbors per nitrogen atom as a function of the [N]/[Si] ratio.

TABLE IV. Assignments, line parameters, and oscillator-strength factors of the six components of local Si—H stretching modes in a-$Si_xN_yH_z$ alloys.

ω_{max} (cm^{-1})	2005	2065	2082	2140	2175	2220
FWHM (cm^{-1})	95	105	100	105	80	125
Configuration	(HSi Si_3)	(H_2Si Si_2)	(HSi NSi_2)	(HSi N_2Si) (H_2Si NSi)	(H_2Si N_2)	(HSi N_3)
K (10^{19} cm^{-2})	7	11	17	11	40	20

genated silicon units can be determined and the resulting relative fractions of nitrogen atoms are plotted against the [N]/[Si] ratio in Fig. 17(b). The experimental dispersion notwithstanding, clear trends are observed at low nitrogen contents where more than two out of three silicon neighbors of a given nitrogen atom are monohydrogenated. An extrapolation of this behavior to the doping range ([N]/[Si] $< 1/100$) yields a preferential $N(SiH)_3$ configuration for almost all nitrogen impurities. This tendency is strongest in films where the Si—N asymmetric stretch absorption profile is distinct from that of samples with higher N contents (see Sec. II). A similar boron-hydrogen spatial correlation has been detected in boron-doped a-Si:H by nuclear magnetic resonance,[19] so that its "chemical" origin is either to be found in common features of the chemistry of boron and nitrogen, or in the strain reduction (or structural relaxation) brought by a local III-III formation with satellites III-IV sites as compared to an isolated III-IV configuration in an a-Si:H matrix. Up to [N]/[Si] $= 1.1$, each nitrogen atom has at least one monohydrogenated nearest neighbor, a result that should be taken into account when the variations with [N]/[Si] of the electronic and optical properties of these alloys are studied in some detail, or when a model of the Si—N stretching vibration is proposed.

VI. CONCLUSION

The results of this experimental determination of the atomic composition, bond concentrations, and first-neighbor configuration statistics of a-$Si_xN_yH_z$ have led us to draw the following conclusions.

(i) The [N]/[Si] solid-state ratio of the PECVD samples (as determined by elastic recoil detection) followed a square-root dependence on $[NH_3]/[SiH_4]$ gas ratio over most of the preparation range. Semiempirical derivations of [N]/[Si] from refractive-index measurements were found to be quite reliable. On the contrary, XPS determinations of this ratio are not at all straightforward, since the mean-free-path ratio $\lambda(N\ 1s)/\lambda(Si\ 2p)$ varies with the composition of the dielectric.

(ii) Assuming a complete valence satisfaction, we proposed original calibrations of most of the nonshifting ir-absorption bands observed in the 600–3600-cm^{-1} range for these alloys: the oscillator-strength factor of the NH wag-rocking (stretching) mode near 1175 cm^{-1} (3335 cm^{-1}) was $(2.1\pm0.2)\times10^{19}$ cm^{-2} $[(1.2\pm0.3)\times10^{20}$ $cm^{-2}]$, and that of the N—H_2 bending (stretching) mode near 1540 cm^{-1} (3445 cm^{-1}) was estimated at $(3.8\pm0.4)\times10^{20}$ cm^{-2} $[(5\pm0.5\times10^{20}$ $cm^{-2})]$, while a calibration factor of $(1.3\pm0.2)\times10^{19}$ cm^{-2} was determined for the Si—N asymmetric stretch broad band in the $0.01 \leq [N]/[Si] \leq 0.8$ range where its peak frequency is constant. The peak frequencies, typical full width at half maximum (FWHM), and assignments of the six components of Si—H stretching-mode absorption band are summarized in Table IV along with their oscillator-strength factors. The factors of shifting bands showed strong variations with composition. At low N contents hydrogen bonding occurred preferentially on silicon as expected in a random alloy. At higher nitrogen concentration, strong "chemical" effects promoted the predominance of bridging NH units.

(iii) The statistics of hydrogenated configurations were determined for the first time in such a ternary alloy. The results of this original quantitative bonding analysis show that the $[SiH]/[SiH_2]$ ratio is about that of the nitrogen-free sample up to [N]/[Si] $= 0.4$, and that the total amounts of di-, mono-, and unhydrogenated silicon and nitrogen atoms are roughly equal to those expected from a description of our alloy as a continuous random network over the whole composition range. The most striking chemical effect was observed at low nitrogen contents where more than two out of three silicon neighbors of a given nitrogen atom are monohydrogenated. Up to [N]/[Si] $= 1.1$, each nitrogen atom was found to have at least one monohydrogenated silicon nearest neighbor. As weaker but similar effects have been observed in PECVD (Ref. 19) heavily boron-doped a-Si:H films, we believe these second nearest-neighbor correlations to be a general feature of III-IV hydrogenated amorphous alloys, independent of the solid-state incorporation law of the impurity of the tetrahedrally bonded network. More generally, the concentrations of hydrogenated tetrahedra are shown to be at least as important as those of unhydrogenated sites, and we feel that these hydrogenated configurations should not be left out in the calculations of the optical properties of Si-based PECVD alloys.[85,86] Finally, for [N]/[Si] greater than 0.6, the bonding geometry of nitrogen atoms was shown to be very similar to the planar site observed in the β phase of crystalline Si_3/N_4. This brings further support to the common hypothesis of tight-binding studies[4,85] of this amorphous alloy.

ACKNOWLEDGMENTS

Grateful thanks are expressed to C. Chaussat and P. Deroux Dauphin, who prepared most of the samples used for this study, as well as to T. A. Nguyen Tan, who performed the XPS measurements. Critical reading of the manuscript by A. Deneuville and D. Jousse is also acknowledged. This work is a result of the France-Quebec Scientific Cooperation Program.

*On leave from Vanier College, Montréal (PQ), Canada.
[1]T. Makino, J. Electrochem. Soc. **130**, 450 (1983).
[2]W. A. P. Claassen, W. G. J. N. Valkenburg, F. H. P. M. Harbraken, and Y. Tamminga, J. Electrochem. Soc. **130**, 2419 (1983).
[3]N. Piggins, E. A. Davis, and S. C. Bayliss, J. Non-Cryst. Solids **97&98**, 1047 (1987).
[4]J. Robertson, Philos. Mag. B **44**, 215 (1981).
[5]H. R. Philipp, J. Phys. Chem. Solids **32**, 1935 (1971).
[6]H. R. Philipp, J. Electrochem. Soc. **120**, 295 (1973).
[7]D. E. Aspnes and J. B. Theeten, J. Appl. Phys. **50**, 4928 (1979).
[8]T. S. Eriksson and C. G. Granqvist, J. Appl. Phys. **60**, 2081 (1986).
[9]F. G. Bell and L. Ley, J. Non-Cryst. Solids **97&98**, 1007 (1987).
[10]R. Kärcher, L. Ley, and R. L. Johnson, Phys. Rev. B **30**, 1896 (1984).
[11]E. Sacher and N. S. McIntyre, Phys. Rev. B **33**, 2845 (1986).
[12]R. Kärcher, L. Ley, and R. L. Johnson, Phys. Rev. B **33**, 2847 (1986).
[13]E. Bustarret and T. A. Nguyen Tan (unpublished).
[14]L. Kubler, R. Haug, E. K. Hlil, D. Bolmont, and G. Gewinner, J. Vac. Sci. Technol. A **4**, 2323 (1986).
[15]N. Voke and J. Kanicki, Mater. Res. Soc. Symp. Proc. **68**, 175 (1986).
[16]S. Furukawa, N. Matsumoto, T. Toriyama, and N. Yabumoto, J. Appl. Phys. **58**, 4658 (1985).
[17]D. V. Tsu, G. Lucovsky, and M. J. Mantini, Phys. Rev. B **33**, 7069 (1986).
[18]D. Jousse, E. Bustarret, A. Deneuville, and J. P. Stoquert, Phys. Rev. B **34**, 7031 (1986).
[19]J. B. Boyle, S. E. Ready, and C. C. Tsai, J. Non-Cryst. Solids **97&98**, 345 (1987).
[20]H. Yokomichi and K. Morigaki, Solid State Commun. **63**, 629 (1987).
[21]R. A. Street, J. Kakalios, C. C. Tsai, and T. M. Hayes, Phys. Rev. B **35**, 1316 (1987).
[22]S. T. Pantelides, J. Non-Cryst. Solids **97&98**, 79 (1987).
[23]M. Maeda and H. Nakamura, J. Appl. Phys. **55**, 3068 (1984).
[24]S. Hasegawa, H. Anbutu, and Y. Kurata, J. Non-Cryst. Solids **97&98**, 1043 (1987).
[25]J. F. Curie, P. Depelsenaire, S. Galarneau, J. L'Ecuyer, R. Grosleau, J. C. Bruyère, and A. Deneuville, J. Phys. (Paris) Lett. **42**, L373 (1981).
[26]C. Chaussat, E. Bustarret, J. C. Bruyère, and R. Groleau, Physica B + C **129B**, 215 (1985).
[27]F. H. P. M. Habraken, R. H. G. Tijhaar, W. F. van der Weg, A. E. T. Kuiper, and M. F. C. Willemsen, J. Appl. Phys. **59**, 447 (1986).
[28]J. Gyulai, O. Meyer, J. W. Mayer, and V. Rodriguez, Appl. Phys. Lett. **16**, 232 (1970).
[29]H. J. Stein, V. A. Wells, and R. E. Hampy, J. Electrochem. Soc. **126**, 1750 (1979).
[30]H. L. Hwang, C. C. Hwu, J. C. Liue, and H. H. Lin, Appl. Phys. Lett. **41**, 844 (1982).
[31]A. J. Lowe, M. J. Powell, and S. R. Elliott, J. Appl. Phys. **59**, 1251 (1986).
[32]R. Hezel and N. Lieske, J. Appl. Phys. **53**, 1671 (1982).
[33]Y. Kojima, S. Narikawa, T. Matsuyama, E. Imada, H. Nojima, T. Hayakawa, and S. Ehara, Mater. Res. Soc. Symp. Proc. **49**, 203 (1985).
[34]S. Hasegawa, T. Tsukao, and P. C. Zalm, J. Appl. Phys. **61**, 2916 (1987).
[35]T. Noguchi, S. Usui, A. Sawada, Y. Kanoh, and M. Kikuchi, Jpn. J. Appl. Phys. **21**, L485 (1982).
[36]A. Morimoto, I. Kobayashi, M. Kumeda, and T. Shimizu, Jpn. J. Appl. Phys. **25**, L752 (1986).
[37]R. Groleau, S. C. Gujrathi, and J. P. Martin, Nucl. Instrum. Methods **218**, 11 (1983).
[38]K. J. Gruntz, L. Ley, and R. L. Johnson, Phys. Rev. B **24**, 2069 (1981).
[39]V. I. Nefedov, N. P. Sergusin, I. M. Band, and M. B. Trzhskovskaya, J. Electron Spectrosc. Relat. Phenom. **2**, 383 (1973).
[40]S. H. Scofield, J. Electron Spectrosc. Relat. Phenom. **8**, 129 (1976).
[41]H. Ibach, in *Electron Spectroscopy for Surface Analysis,* Vol. IV of *Topics in Current Physics* (Springer, Berlin, 1977), p. 7.
[42]C. C. Lu, T. A. Carlson, F. B. Malik, T. C. Tucker, and C. W. Nestor Jr., At. Data **3**, 1 (1971).
[43]A. Iqbal, W. B. Jackson, C. C. Tsai, J. W. Allen, and G. W. Bates, Jr., J. Appl. Phys. **61**, 2947 (1987).
[44]D. L. Smith, A. S. Alimonda, Chau Chen-Chen, W. B. Jackson, and B. Wacker, Mater. Res. Soc. Symp. Proc. (to be published).
[45]M. Stutzmann, Mater. Res. Soc. Symp. Proc. **70**, 203 (1986).
[46]E. Bustarret, F. Vaillant, and B. Hepp, Mater. Res. Soc. Symp. Proc. (to be published).
[47]B. Abeles, L. Yang, P. D. Persans, H. S. Stasiewski, and W. Lanford, Appl. Phys. Lett. **48**, 168 (1986).
[48]M. Maeda and H. Nakamura, J. Appl. Phys. **58**, 484 (1985).
[49]Yu. N. Volgin, G. P. Dubrovskii, and Yu. I. Ukhanov, Sov. Phys.—Solid State **17**, 1089 (1975).
[50]J. P. Luongo, J. Electrochem. Soc. **130**, 1560 (1983).
[51]N. Wada, S. A. Solin, J. Wong, and S. Prochazka, J. Non-Cryst. Solids **43**, 7 (1981).
[52]E. A. V. Ebsworth, J. R. Hall, M. J. McKillop, D. C. McKean, N. Sheppard, and L. A. Woodward, Spectrochim. Acta **13**, 202 (1958).
[53]F. A. Miller, J. Perkins, G. A. Gibbon, and B. A. Swisshelm, J. Raman Spectrosc. **2**, 93 (1974).
[54]M. L. Naiman, C. T. Kirk, R. J. Aucoin, F. L. Terry, P. W. Wyatt, and S. D. Senturia, J. Electrochem. Soc. **131**, 637 (1984).
[55]M. Achard and F. Ferrieu (unpublished).
[56]A. D. Yadav and M. C. Joshi, Thin Solid Films **59**, 313 (1979).
[57]H. J. Stein, Appl. Phys. Lett. **43**, 296 (1983).
[58]G. Lucovsky, S. S. Chao, J. Yang, J. E. Tyler, and W. Czubatyj, J. Vac. Sci. Technol. **A2**, 353 (1984).
[59]M. Bensouda, M. C. Habrard and J. C. Bruyère (unpublished).
[60]D. Jousse, J. Kanicki, J. Batey, and Y. Cros (unpublished).
[61]A. Marchand, M. T. Forel, F. Metras, and J. Valade, J. Chim. Phys. (Paris) **61**, 343 (1964).
[62]S. Narikawa, Y. Kojima, and S. Ehara, Jpn. J. Appl. Phys. **24**, L861 (1985).
[63]Y. Itoh, T. Nozaki, T. Masui, and T. Abe, Appl. Phys. Lett. **47**, 488 (1985).
[64]A. Morimoto, Y. Tsujimura, M. Kumeda, and T. Shimizu, Jpn. J. Appl. Phys. **24**, 1394 (1985).
[65]G. Sasaki, M. Kondo, S. Fujita, and A. Sasaki, Jpn. J. Appl. Phys. **21**, 1394 (1982).
[66]H. Watanabe, K. Katoh, and M. Yasui, Thin Solid Films **106**, 263 (1983).
[67]C. J. Fang, K. J. Gruntz, L. Ley, M. Cardona, F. J. Demond, G. Muller, and S. Kalbitzer, J. Non-Cryst. Solids **35&36**, 255 (1980).
[68]W. A. Lanford and M. J. Rand, J. Appl. Phys. **49**, 2473 (1978).
[69]P. S. Peercy, H. J. Stein, B. L. Doyle, and S. T. Picraux, J. Electron. Mater. **8**, 11 (1979).

[70]V. J. Kapoor, R. S. Bailey, and H. J. Stein, J. Vac. Sci. Technol. A **1**, 600 (1983).
[71]S. Fujita, N. S. Zhou, and A. Sasaki, Jpn. J. Appl. Phys. **22**, L100 (1983).
[72]Y. Cros and J. C. Rostaing, in *Proceedings of the European Materials Research Society—Dielectric Layers in Semiconductors,* edited by G. G. Bentini (Les Editions de Physique, Les Ulis, 1986), p. 77.
[73]A. G. Dias, E. Bustarret, and R. C. Da Silva, in *The Physics and Technology of Amorphous SiO_2,* edited by R. Devine (Plenum, New York, 1988).
[74]T. Aiyama, T. Fukunaga, K. Niihara, T. Hirai, and K. Suzuki, J. Non-Cryst. Solids **33**, 131 (1979).
[75]A. K. Sinha and E. Lugujjo, Appl. Phys. Lett. **32**, 245 (1978).
[76]M. Maeda and Y. Arita, J. Appl. Phys. **53**, 6852 (1982).
[77]F. Betts, A. Bienenstock, and S. R. Ovshinsky, J. Non-Cryst. Solids **4**, 554 (1970).
[78]G. Lucovsky, F. L. Galeener, R. H. Geils, and R. C. Keezer, in *The Structure of NonCrystalline Materials,* edited by P. H. Gaskell (Taylor and Francis, London, 1977), p. 127.
[79]G. Lucovsky and T. M. Hayes, in *Amorphous Semiconductors,* Vol. 36 of *Topics in Applied Physics,* edited by M. H. Brodsky (Springer, Berlin, 1980), p. 215.
[80]H. R. Philipp, J. Non-Cryst. Solids **8-10**, 627 (1972).
[81]W. R. Knolle and J. W. Osenbach, J. Appl. Phys. **58**, 1248 (1985).
[82]J. C. Rostaing, Y. Cros. S. C. Gujrathi, and S. Poulain, J. Non-Cryst. Solids **97&98**, 1051 (1987).
[83]H. R. Phillipp, footnote on p. 1943, Ref. 6.
[84]E. Bustarret and E. Morgado, Solid State Commun. **63**, 581 (1987).
[85]L. Martin-Moreno, E. Martinez, J. A. Vergés, and F. Yńdurin, Phys. Rev. B **35**, 9683 (1987).
[86]K. Mui and F. W. Smith, Phys. Rev. B **35**, 8080 (1987).